

Research Paper

The Effect of Rotational Speeds on the Microstructural and Mechanical Properties of Friction Stir Welded Dissimilar Aluminum Alloy Plates

Tankiso Lawrence NGAKE*, Kadephi Vuyolwethu MJALI

Walter Sisulu University, Department of Mechanical Engineering
Private Bag X3182, Butterworth, 4960, Eastern Cape, South Africa
e-mail: kvmjali@wsu.ac.za

*Corresponding Author e-mail: tngake@wsu.ac.za

The aim of this study is to investigate the effects of rotational speed on the quality of welds, microstructure, and mechanical properties in friction stir welding of dissimilar aluminum alloys (AA5083 and AA6082). Different samples were produced by varying the rotational speeds to 900, 1000, 1130, and 1260 rpm. The microstructure of the weld joints was evaluated by optical microscopy, while microhardness and tensile stress were examined using a microhardness tester and tensile tester. The microstructural analysis indicates fine equiaxed recrystallized grains in the stir zone for all the samples, regardless of rotational speeds. However, the macrographs indicated the development of voids with increasing rotational speeds. The lowest microhardness was observed in the stir zone for all the samples. The ultimate tensile stress decreased as rotational speed increased. Overall, the lowest rotational speed of 900 rpm yielded optimal results, with minimal defects and higher tensile strength.

Keywords: friction stir welding; aluminum alloy; microstructure; mechanical properties.

1. INTRODUCTION

In the realm of advanced welding techniques, friction stir welding (FSW) has emerged as a cutting-edge method for joining dissimilar aluminum alloys. FSW joins materials using frictional heat generated between a rotating tool and the materials being welded. The technique was first developed by The Welding Institute (TWI), in the UK in 1991 [1]. FSW has since found extensive applications in the aerospace, maritime, automotive, and railway industries [2]. As a result, recent research has focused on fundamental aspects such as rotational speed, weld nugget formation, microstructure, mechanical properties, and other key process parameters. Unlike traditional welding methods, FSW does not involve melting the materials, which helps reduce defects such as porosity

and cracking in the weld. Moreover, FSW offers several advantages over fusion welding of aluminum. Fusion welding often results in the formation of oxide layers, high thermal conductivity, and shrinkages during solidification process as a result of differences in the coefficient of thermal expansion. However, such problems are eliminated with FSW. Furthermore, the distortions and residual stresses in weld nugget are reduced by FSW as well.

In the automobile, aerospace, and railway industries, weight reduction is important for fabricating heavy machine parts due to the limitations in the strength-to-weight ratio [3]. Materials such as copper alloys steels, wrought iron, titanium and magnesium alloys are replaced by aluminum and its alloys because of their superior properties. Researchers have extensively explored the impact of FSW and its processing parameters on the microstructure and mechanical properties of aluminum alloys. HIRATA *et al.* [4] investigated the influence of heat flow during FSW on grain size and formability in 5083 Al alloy. Their findings revealed that the grain size in the stir zone (SZ) decreased with the decrease in friction heat flow. Moreover, the ductility in the welded alloy increased with reduced friction heat flow. Additionally, formability was improved due to grain size refinement in the SZ.

Similarly, WAN *et al.* [5] studied the effect of varying welding speed on the mechanical properties of 6082-T6 Al alloy. Their results indicated that tensile strength of joints increased with elongation decreased as welding speed was raised from 10 to 200 mm/min. Moreover, defect-free joints were obtained at lower welding speeds. CAVALIERE *et al.* [6] investigated the influence of both rotating speed and welding speed on the mechanical properties of FS-welded Al alloy. They observed that ductility of the material decreased with increasing rotational speed and welding speed. The tensile strength was highest at higher rotating and welding speeds. Fine microstructures were observed in all welding conditions. The microstructure in the SZ was changed by dynamic recrystallization during FSW. The microstructure in the SZ is influenced by FSW parameters. Higher rotational speeds led to finer grain structure and improved mechanical properties, such as higher tensile strength and hardness [7]. Additionally, microstructural analysis showed good diffusion and interlocking between dissimilar metals, indicating a strong bond between the aluminum alloy plates. This research demonstrates that control of rotational speed during FSW of dissimilar aluminum alloy plates can have a significant impact on the resulting microstructure and mechanical properties.

The FSW process has proven its effectiveness for joining dissimilar materials such as aluminum and stainless steel. However, further research is needed to understand the impact of process parameters, specifically rotational speeds, on the microstructure and mechanical properties of friction stir welded dissimilar aluminum alloy plates, specifically focusing on 5083-H113 and 6082-T651 alloys.

To address this research gap, our study aims to investigate the effect of rotational speeds on the microstructure and mechanical properties of FSW joints for these dissimilar aluminum alloy plates. In order to achieve this, a comprehensive experimental study was conducted. Understanding the impact of different rotational speeds on the weld quality is crucial for optimizing the welding process and ensuring the structural integrity of the final product.

This study presents a comprehensive analysis and characterization of mechanical properties such as tensile strength and microhardness. By varying rotational speeds during the welding process, the research explores how changes in these parameters influence the overall performance and durability of the welded joint. Additionally, the article discusses the microstructural changes induced by the welding process, providing valuable insights into the relationship between welding parameters and mechanical behavior.

This research not only contributes to the existing body of knowledge on FSW but also practical implications for industries such as aerospace and automotive manufacturing, where the use of dissimilar aluminum alloys is prevalent. By identifying the optimal conditions for producing high-quality welds with these specific alloys, the study paves the way for more efficient production methods and the development of reliable welded structures.

2. EXPERIMENTAL

2.1. Materials

In this study, a 6082-T651 aluminum plate with dimensions of $100 \times 20 \times 6$ mm and a 5083-H113 aluminum plate with dimensions of $100 \times 20 \times 5$ mm were utilized, with the chemical of the base materials shown in Table 1.

Table 1. Chemical composition (weight %) of the base materials.

Alloy	Mn	Fe	Cu	Mg	Si	Zn	Cr	Ti	Al
A5083	0.40–1.00	0.40	0.10	4.00–4.90	0.40	0.25	0.05	0.15	Bal
A6082	0.40–1.00	0.50	0.10	0.60–1.20	0.70–1.30	0.20	0.25	0.10	Bal

2.2. FSW

Figure 1a illustrates the FSW process setup used in this study. The FSW was performed using a Pinnacle PK-GRSM-V milling machine. The metal plates to be joined were clamped onto a rigid backing body (as shown in Fig. 1a) to prevent any movement during the welding process. Several welding parameters, including tool rotational speed, welding speed, and tool pin profile, influence material flow behavior during FSW. In this experiment, the FSW tool was equipped

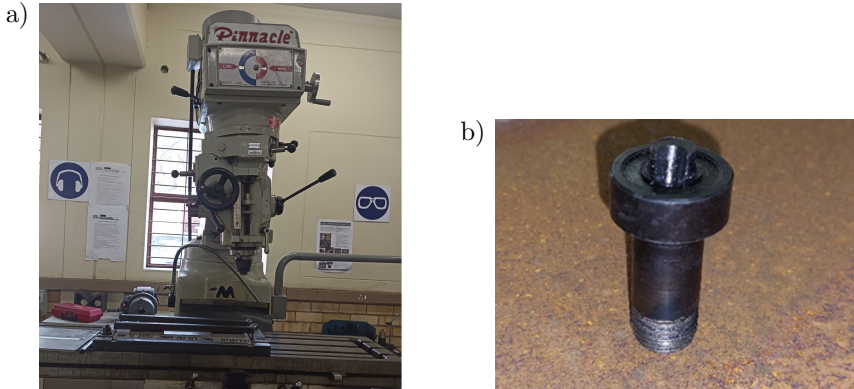


FIG. 1. FSW Platform (a) Pinnacle PK-GRSM-V milling machine used for the FSW process, (b) FSW tool with cylindrical threaded pin.

with a cylindrical shoulder with a diameter of 25.4 mm and a threaded cylindrical pin with a cut as shown in Fig. 1b. The pin diameter was 2.5 mm, with a length of (provide pin length). The A5083 plates were always positioned on the advancing side (AS) of the welding tool, while the A6082 were placed on the retreating side (RS). The FSW tool moved 90 mm along the joint line, parallel to the rolling direction. Four rotational speeds of 900, 1000, 1130, and 1260 rpm were investigated in this study. Sample naming used throughout the paper is shown in Table 2, where sample 5 is the unwelded A5083 and sample 6 represents the unwelded A6082. The welding speed, plunge depth, and tilt angle were kept constant at 120 mm/min, 0.5 mm, and 4° , respectively. The rotating tool pin was slowly pushed into the seam axially until the tool shoulder came into contact with the surface of the material, which generated frictional heat that locally softened the material around the pin. The penetration depth of the tool shoulder into the plates was about 0.5 mm, and the axial position of the pin tool remained constant while it traversed along the seam at a constant speed. The welded joints showed a smooth surface finish when evaluated visually.

Table 2. Tensile samples' dimensions and rotational speeds.

Sample	FSW rotational speed [rpm]	Average width [mm]	Average thickness [mm]
1	900	12.48	4.97
2	1000	12.49	4.96
3	1130	12.54	4.96
4	1260	14.44	4.99
5	–	12.57	5.03
6	–	12.62	5.99

2.3. Microstructure

The samples were cut perpendicular to the weld direction using waterjet cutting. Subsequently, they were cold-mounted using ClaroCit powder and liquid in a ratio of 20:12 for 20 minutes. Grinding was performed manually using 120, 600, and 1200 SiC-bonded grinding papers. Polishing was carried out using an MD-Chem polishing disk with a 3 μm colloidal silica suspension. After polishing, the samples were etched in 1% NaOH for one minute to reveal the microstructure. The microstructure was examined using an Olympus DSX510 optical microscope at 100 \times magnification for macrostructures and 500 \times magnification for microstructures to obtain clear images.

2.4. Tensile

The tensile samples were cut into a dog bone shape, transverse to the weld direction, using waterjet cutting. They were then machined to the required dimensions (as depicted in Fig. 2) to prepare the tensile specimens according to ASTM standards. The tensile specimens were cut so that the weld was centered in the gauge section, with the tensile axis was normal to the welding direction. Due to fact that the samples consisted of dissimilar materials, ten width measurements (from the top and bottom) and five thickness measurements were taken from each FSW sample, and an average was calculated and is presented in Table 2. The averaging of these measurements was conducted to compensate for the uneven samples resulting from the cutting process. Sample 5 corresponds to the Al-5083 parent material, and Sample 6 is the Al-6082 parent material. The tensile tests were performed at room temperature using an Instron 3367 Tensile Tester at a crosshead speed of 2.9 mm/min. Figure 3b shows the samples after the tensile tests.

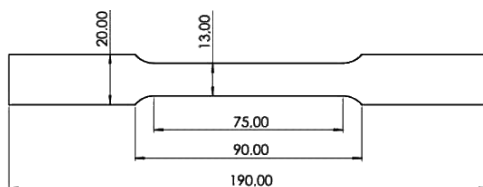


FIG. 2. Geometry and dimensions (in mm) of the tensile samples.

2.5. Hardness

The samples used for microstructure analysis were also utilized for microhardness testing. The microhardness of the samples was determined from the cross-section perpendicular to the weld direction using the Emco Test DuraScan

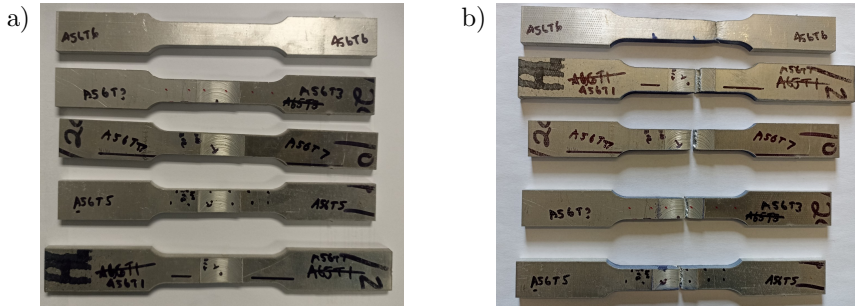


FIG. 3. Tensile samples: a) before tensile tests, b) after tensile tests.

micro-hardness tester, employing the Vickers hardness (HV) 0.5 method with a testing force of 500 g, following the ASTM E9 standard. Hardness measurements were positioned along a straight line in the middle of the sample's thickness and were taken in six different zones: A5083 base material (PM1), which is on the AS; heat affected zone on the AS (HAZ-1), stir zone (SZ), thermo-mechanical affected zone (TMAZ) clearly visible on the RS, and not so distinctly visible on the AS, heat affected zone on the RS (HAZ-2), and A6082 base material (PM2), which is on the RS, as indicated in Fig. 4. Three indents were created in each zone, and the average values are presented in Table 3.

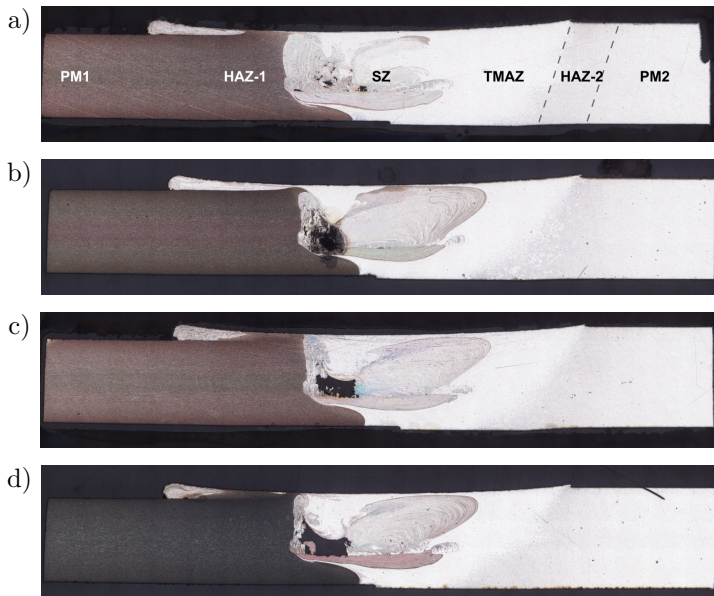


FIG. 4. Cross-sectional macrographs of the FSW Al-5083 and 6082 at various rotational speeds: a) 900 rpm, b) 1000 rpm, c) 1130 rpm, and d) 1260 rpm.

Table 3. Hardness measurements in [HV] at various zones across the weld.

Sample	PM1	HAZ-1	SZ	TMAZ	HAZ-2	PM2
1	75.9	73.2	61.6	64.9	65.8	63.5
2	80.0	76.7	59.9	71.6	72.9	68.8
3	74.7	72.2	60.5	73.3	71.5	70.4
4	81.7	81.5	66.9	73.4	71.3	75.8

3. RESULTS AND DISCUSSION

3.1. Macro- and microstructure

Figure 4 presents the macrographs of FSW samples processed at various rotational speeds, captured through optical microscopy at $100\times$ magnification. The macrographs reveal six distinct zones, as shown in Fig. 4a. PM1 represents the 5083 parent material located on the AS, while HAZ-1 is the heat-affected zone on the 5083 side. The SZ is located at the center of the weld joint and features a nugget-shaped region where both materials are thoroughly mixed. TMAZ denotes the thermo-mechanically affected zone, while HAZ-2 and PM2 represent the heat-affected zone on the 6082 side and the 6082 parent material on the RS, respectively. The TMAZ is formed through a combination of friction between the tool shoulder and the plate surface, as well as plastic deformation of the material in contact with the stir pin, as described in [8].

As shown in Fig. 4, no distinct separation between the HAZ and TMAZ was observed on the 5083 side (AS), whereas the boundary between these zones was clearly visible on the 6082 side (RS). This finding contrasts with the observations of MISHRA *et al.* [9], where the distinction between the HAZ and TMAZ was more pronounced on the AS. At a lower rotational speed of 900 rpm, the nugget zone was centrally located within the weld joint. However, at higher rotational speeds, it shifted toward the retreating side. Additionally, the SZ was broader at the top than at the bottom, indicating limited downward material flow. The material flow was found to be directly influenced by the tool rotation [10].

Voids were observed in the nugget zone toward the AS, as shown in Fig. 4b–d, with their prevalence increasing at higher rotational speeds. This can be attributed to the increased frictional heat generated by the tool's threaded pin at higher speeds, resulting in higher heat input into the SZ. Excessive heat softens the material excessively, making it overly plasticized and impairing material flow. Consequently, the softened material fails to fully fill voids. Additionally, inadequate material consolidation may occur as the rapid tool movement at higher speeds does not allow enough time for the plasticized material to consoli-

date behind the tool. Uneven heat distribution across the weld zone may further contribute to void formation, with over-softened areas forming near the tool and cooler, less plasticized regions further away. Similar defects were reported by [4], who attributed their formation to metal flow driven by shoulder extrusion and pin stirring. The wider shoulder creates a stirring effect that extends into the plate. BERNARD and HATTHING [11] also observed that reducing the rotational speed and increasing the downforce significantly reduced void formation.

The macrographs also revealed interleaving bands, known as onion rings, within the nugget zone – a characteristic feature of the FSW process [12]. This microstructure arises from the material flow patterns around the tool, with alternating layers of each alloy forming a vortex-like structure. The formation of onion rings is attributed to frictional heat generated by tool rotation and the cylindrical extrusion of material toward the RS. It has been reported that the spacing between onion rings corresponds to the tool's forward movement during one rotation [13].

The weld joint cross-sections of the FSW samples were analyzed using optical microscopy at 500x magnification to obtain detailed images of the microstructures, as shown in Figs. 5–7. Figure 5 presents the microstructures of the parent materials PM1 and PM2. PM1 exhibits a relatively uniform grain size, slightly elongated along the rolling direction, while PM2 shows a hybrid microstructure comprising fine, partially recrystallized grains and non-recrystallized grains. These findings align with previously reported results in the literature [14].

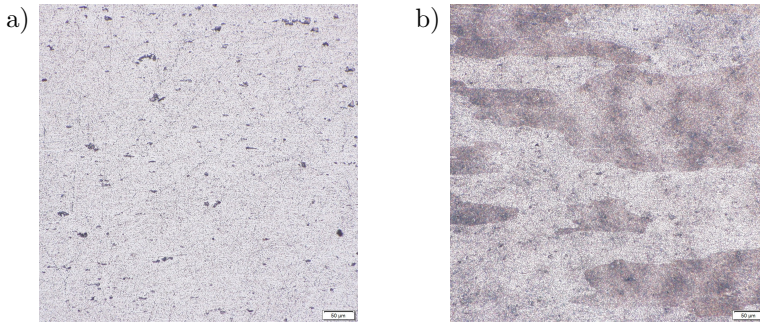


FIG. 5. Microstructures of the parent materials: a) PM1, b) PM2.

The primary factors influencing microstructural changes include heat generation, material flow, and dynamic recrystallization. Due to the differing thermal and mechanical properties of the 5xxx series (Al-Mg alloys) and 6xxx series (Al-Mg-Si alloys), variations in rotational speed affect their microstructures differently, as illustrated in Figs. 6 and 7.

Figure 6 highlights the SZ, which consists of fine, inhomogeneous, equiaxed recrystallized grains. These grains form under conditions of high temperature

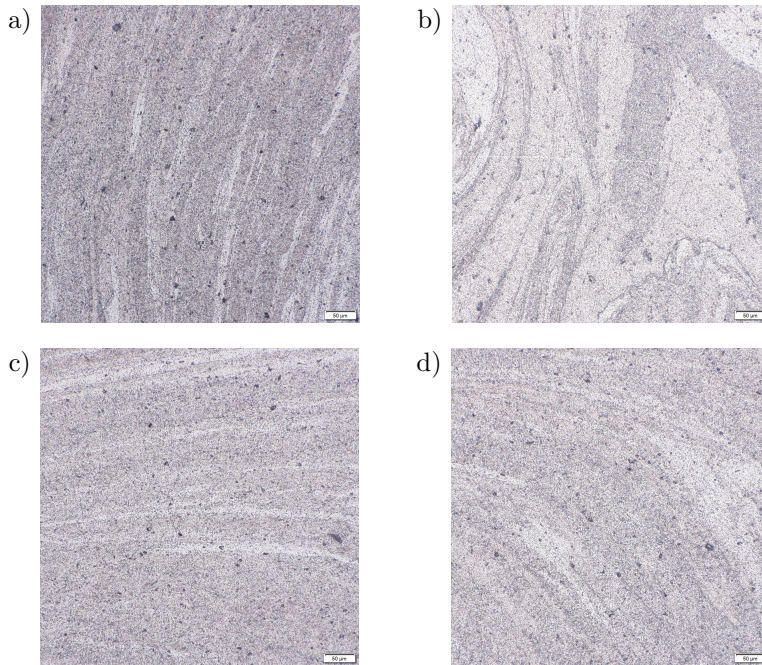


FIG. 6. Microstructures of the SZ at: a) 900 rpm, b) 1000 rpm, c) 1130 rpm, and d) 1260 rpm.

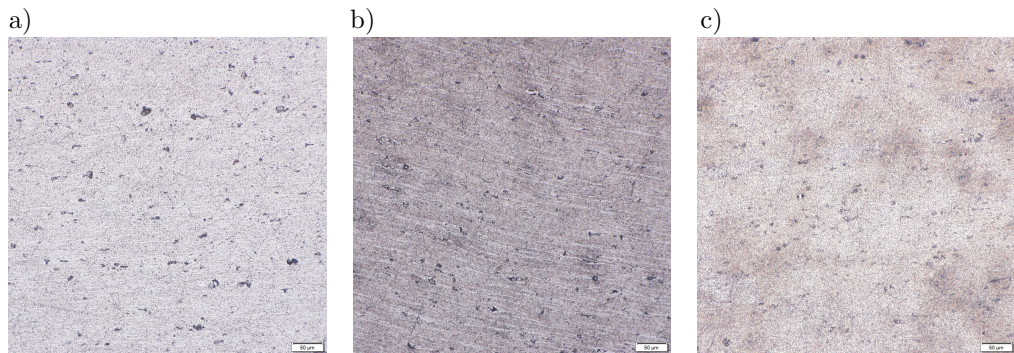


FIG. 7. Microstructures of: a) HAZ-1, b) TMAZ, and c) HAZ-2.

and significant deformation, driven by the stirring action of the tool pin. At higher rotational speeds, elevated temperatures promote dynamic recrystallization, resulting in finer equiaxed grains, as seen in Fig. 6a. The grains bend around the nugget zone due to the intense deformation induced during welding. Samples 2 and 4 exhibit coarser grains compared to Samples 1 and 3. Figure 6b shows inadequate mixing of the two alloys, leading to a sharp boundary between the 5xxx and 6xxx alloys with minimal diffusion of alloying elements across the

interface. According to [4], grain size in the SZ decreases with a reduction in rotational speed, demonstrating the impact of rotational speed on the resultant microstructure.

Figure 7 depicts the microstructures of HAZ-1, TMAZ, and HAZ-2. HAZ-1 shows a grain structure resembling that of PM1, with slightly coarsened grains due to thermal cycling. In contrast, HAZ-2, being closer to the weld center, experiences higher thermal cycle temperatures and longer heating times, resulting in partial grain recovery in this region. The TMAZ features a hybrid microstructure consisting of both deformed, elongated grains and fine recrystallized grains. This zone undergoes plastic deformation and elevated temperatures, causing grains to elongate along the direction of material flow.

The microstructural differences in the TMAZ arise from the contrasting properties of the 5xxx and 6xxx alloys. The 5xxx alloy, being strain-hardened, retains more of its elongated grain structure in the TMAZ at lower temperatures, where reduced recrystallization occurs (e.g., at lower rotational speeds). At higher rotational speeds, increased temperatures drive more dynamic recovery or partial recrystallization, leading to coarser grains. Conversely, the 6xxx alloy, which relies on precipitation strengthening through Mg_2Si particles, exhibits limited precipitate dissolution under reduced thermal exposure at lower temperatures. This allows some strengthening precipitates to remain intact, with minimal grain coarsening. However, at higher rotational speeds, increased heat input causes Mg_2Si precipitates to dissolve, and they may not fully reform during cooling. This results in reduced strength in the TMAZ. In addition, grain coarsening becomes more pronounced in this region, particularly near the boundary with the SZ, due to the elevated temperatures.

3.2. Microhardness

Microhardness measurements were taken on the cross-section of the weld joint, and the results are presented in Table 4. AA5083 (PM1) shows greater

Table 4. Tensile measurements of the parent and FSW samples.

Sample	Yield stress [MPa]	Maximum force [kN]	Ultimate tensile stress (UTS) [MPa]	Elongation [%]
1	129.06	9.50	153.18	3.43
2	105.91	7.49	120.84	1.78
3	83.79	5.94	95.53	1.64
4	79.69	5.97	82.81	1.51
5	135.89	19.01	300.64	20.65
6	309.46	24.04	318.00	12.50

hardness values with an average of 78.1 HV0.5 compared to AA6082 (PM2), which has an average of 69.6 HV0.5. Similar results were reported in [15]. The results were expected due to high content of magnesium found in 5083 alloy which makes the alloy harder than the 6082 counterpart. The hardness of the PM1 zone was the highest in all the samples, while the SZ was the lowest, as depicted in Fig. 7, indicating the occurrence of thermal softening.

In the RS, the hardness increases from the PM2 zone to the HAZ-2 zone, then decreases towards the SZ. However, on the AS, the hardness decreases from the PM1 towards the HAZ-1 zone and decreases further towards the SZ. This indicates more severe deformation on the AS than on the RS during the welding process. The hardness in the SZ remains rather constant with increasing rotational speed up to 1130 rpm, followed by an approximate increase of 7 HV0.5 at 1260 rpm. During the FSW process of dissimilar materials, the positioning of the materials on either the AS or RS influences the hardness in the SZ. MONI [16] reported an increase of approximately 10 HV when the 6082 is on the AS compared to when it is on the RS.

In Fig. 8, at lower rotational speeds of 900 and 1000 rpm, the hardness in the HAZ is higher than in the TMAZ; however, at higher rotational speeds, the hardness of the TMAZ is higher than that of the HAZ. This increase in hardness values at higher rotational speeds can be attributed to the high density of dislocations induced by the plastic deformation during welding [17]. Sample 4 has the highest hardness across all the weld zones, with the TMAZ hardness being almost the same as in Sample 3, while Sample 1 shows the lowest hardness towards the RS, as shown in Fig. 9. Moreover, Samples 2, 3, and 4 display uniform hardness values in both the TMAZ and HAZ-2 regions. This is a result of partial plastic deformation, the action of the tool, and the high temperature in these two zones, resulting in finer grains.

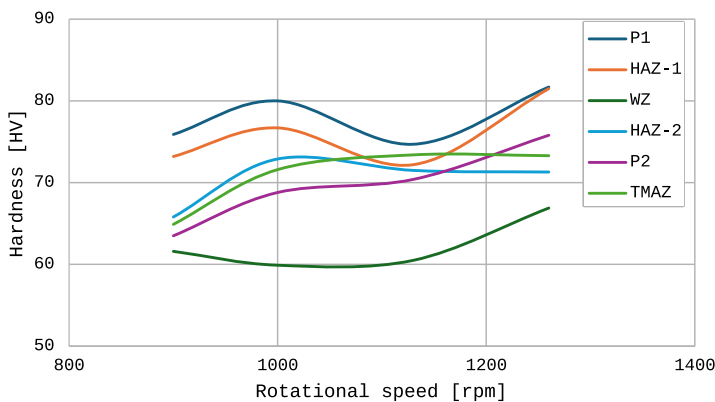


FIG. 8. Comparison of rotational speeds at various SZs.

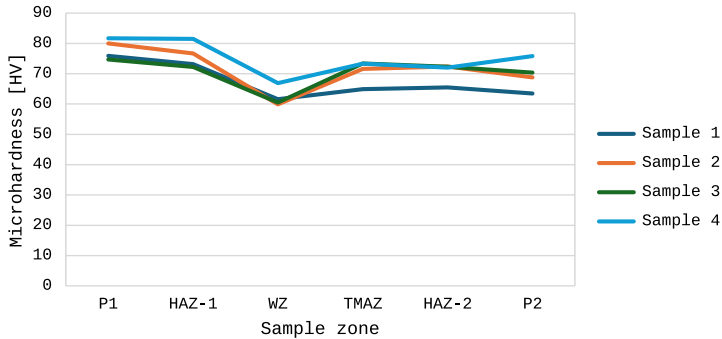


FIG. 9. Microhardness measurements of the FSW samples at different SZs.

The rotational speed of the tool plays a significant role in determining mechanical properties such as hardness in FSW. At higher rotational speeds, more heat is generated due to increased friction, leading to greater thermal softening, especially in the HAZ. This thermal softening reduces hardness due to recrystallization, as indicated in Table 3, especially on the AS. The difference in hardness values between the PM and HAZ is not significantly large, indicating that the HAZ experienced less heat during FSW, resulting in less pronounced microstructural changes. In contrast, the hardness in the TMAZ is influenced by both thermal and mechanical effects. Generally, the low heat input associated with lower rotational speeds results in relatively higher hardness due to reduced thermal softening and limited deformation. However, in this study, the hardness in the TMAZ increases with increasing rotational speed, suggesting that the effect of mechanical deformation outweighed the thermal softening.

Hardness values in the SZ are influenced by recrystallization and grain refinement, both of which are affected by changes in rotational speed. For instance, at lower rotational speeds, the material experiences less heat, and recrystallization may be incomplete or less effective. This results in larger grain sizes and possibly higher hardness, as full grain refinement might not occur. In this study, there is no linear relationship between hardness in the SZ and rotational speed. This indicates that hardness in this zone depends on a balance between grain refinement and avoiding excessive thermal softening. The HAZ typically experiences thermal softening, leading to reduced hardness compared to the PM. However, in this study, the hardness values in HAZ-2 are higher than those in PM2 at rotational speeds of 900 to 1130 rpm. This may be due to precipitation hardening in the A6082 alloy caused by some level of natural aging after welding. This process strengthens the HAZ more than the base material. Another possible explanation could be an overlap between the HAZ and TMAZ, which can lead to higher hardness values in the HAZ. This occurs when the HAZ

experiences more mechanical deformation than expected due to tool geometry or process parameters.

3.3. Tensile

The tensile samples were cut into a dog bone shape transversely to the weld joint using water jet cutting, as illustrated in Fig. 2. The tensile measurements were taken at room temperature with a crosshead speed of 2.9 mm/min, and the results are presented in Table 4. The fracture behavior of both parent materials showed a ductile 45° rupture pattern. The fracture position of the FSW sample was in the weld center (SZ), towards the AS where the void is located, as shown in Fig. 3b. This observation is consistent with the results obtained by THREADGILL *et al.* [18], who indicated that the fracture of FSW joints during tensile testing starts from the weakest point of the weld specimen, typically corresponding to the zone of minimum hardness. The fractures in the FSW samples were characterized by 45° facets of ductile shear rupture, indicating that the stress concentration at defects led to the fracture.

Both the yield stress and tensile stress of the FSW samples decreased with increasing rotational speed, as shown in Table 4 and Fig. 10, respectively. The tensile properties of the weld are influenced by the balance between sufficient heat for good material flow and avoiding excessive heat that weakens the microstructure or causes defects. In general, an optimal rotational speed leads to adequate heat input, ensuring good material flow and a fine-grained microstructure in the SZ, resulting in high tensile strength. However, in the present study, rotational speeds ranging from 1000 to 1260 rpm seemed to create excessive heat, resulting in defects due to poor material flow, leading to reduced tensile strength.

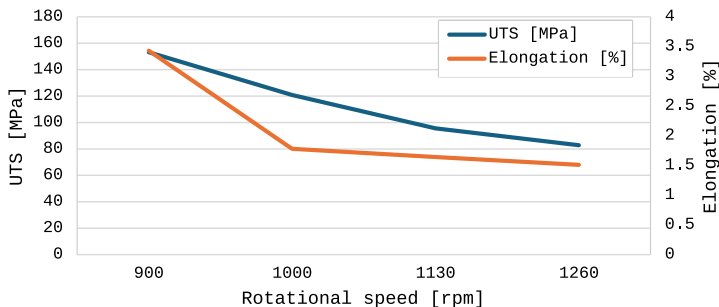


FIG. 10. The ultimate tensile stress of the FSW and parent samples.

The maximum tensile force reached 9.5 kN for the FSW samples, which was observed for Sample 1, as shown in Fig. 11. Samples 3 and 4, with the highest rotational speeds, exhibited the lowest forces of 5.94 and 5.97 kN, respectively.

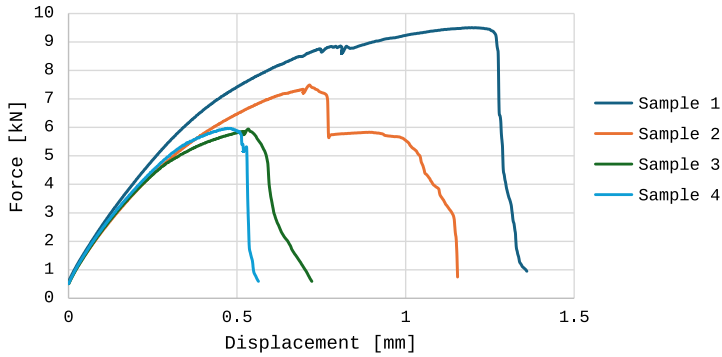


FIG. 11. Force against displacement graph for the FSW samples.

Tensile stress as a function of strain for the FSW samples is shown in Fig. 12. A similar trend of tensile stress and rotational speed was observed with ductility and rotational speed, where ductility decreases with increasing rotational speed. A similar trend was observed by CAVALIERE *et al.* [6] at a welding speed of 56 mm/min, although the trend changed when they increased the welding speed to 80 mm/min. This indicates the important role played by FSW process parameters in improving the mechanical properties of the welded aluminium alloys.

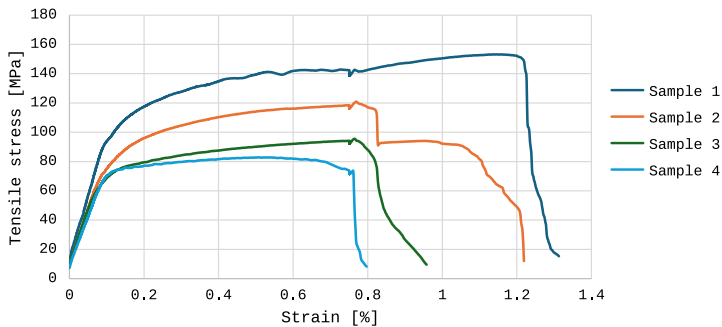


FIG. 12. Stress against strain graph for the FSW samples.

The key factors that influence ultimate tensile stress (UTS) are thermal softening and material flow, which can be controlled by adjusting the heat input. The 5xxx and 6xxx series respond differently to heat input. Excessive heat can reduce the strengthening effects in 6xxx alloys, while 5xxx alloys tend to be more stable under thermal cycling. Therefore, it is important to maintain balanced heat input during FSW of dissimilar alloys. In this study, UTS was directly influenced by heat input as a result of varying rotational speeds. Higher rotational speeds generated excessive heat, which led to voids in the SZ, reducing UTS.

At 900 rpm, optimal heat input was achieved, promoting effective material mixing between the 5xxx and 6xxx alloys. The thermal softening was balanced with sufficient mechanical stirring, enhancing grain refinement and bonding between the dissimilar alloys. This reduced defects and resulted in higher UTS at this rotational speed. UTS and hardness usually show a positive correlation in the SZ due to grain refinement and recrystallization. However, due to the non-linear correlation between hardness and rotational speed observed in this study, it is clear that the results are strongly influenced by weld quality, material flow, and the balance between thermal softening and mechanical deformation. Moreover, ductility is reduced with increasing rotational speed. As mentioned earlier, high rotational speeds cause excessive heat input, leading to potential weld defects and material mixing issues. This result in a loss of mechanical integrity and reduced ductility.

4. CONCLUSIONS

The microstructural and mechanical behaviour of friction stir welded 5083 and 6082 aluminum alloys at four different rotational speeds (900, 1000, 1130, and 1260 rpm) was studied in this work. Rotational speed plays a crucial role in weld quality. Increasing the rotational speed affects material flow, leading to the development of defects. However, good mixing of materials was observed at 900 rpm, leading to reduced voids. Different microstructural changes at different zones resulted in different hardness values in these zones.

In the AS, hardness decreases from the parent material towards the SZ, while in the RS, hardness increases from the parent material to the TMAZ, and then decreases towards the SZ. The tensile properties (yield stress, tensile stress, elongation, and ductility) of the FSW samples decrease with increasing rotational speed, and the maximum tensile strength was found to be 51% of that of the parent material A5083 and 48% of A6082. The tensile fractures occurred in the SZ towards the HAZ on the AS, and the tensile specimens exhibited a 45° ductile failure. The results emphasizes the dependence of quality welds on process parameters. These results can be used to optimize the FSW process for aluminium alloys.

ACKNOWLEDGMENTS

The authors would like to acknowledge the following institutions for their support: Walter Sisulu University, Department of Research and Innovation, for funding, Walter Sisulu University, Department of Mechanical Engineering, and Nelson Mandela University eNtsa Laboratory, Qheberha, South Africa.

DECLARATION OF CONFLICTING INTEREST

The authors declare that there are no known competing financial interests or personal relationships that could have influenced the work reported in this paper.

REFERENCES

1. SANTHOSHKUMAR S., SENTHIL KUMAR K.L., KALIL RAHIMAN M., MATHANKUMAR P., A review on friction stir welding of aluminium alloys and the effects on tool geometry, *IOP Conference Series: Materials Science and Engineering*, **764**(1): 012009, 2020, doi: 10.1088/1757-899X/764/1/012009.
2. MURR L.E., LI Y., TRILLO E., MCCLURE J.C., Fundamental issues and industrial applications of Friction-Stir Welding, *Materials Technology*, **15**(1): 37–48, 2000, doi: 10.1080/10667857.2000.11752854.
3. PAIK J.K., Mechanical properties of friction stir welded aluminium alloys 5083 and 5383, *International Journal of Naval Architecture and Ocean Engineering*, **1**(1): 39–49, 2009, doi: 10.2478/IJNAOE-2013-0005.
4. HIRATA T., OGURI T., HAGINO H., TANAKA T., CHUNG S.W., TAKIGAWA Y., HIGASHI K., Influence of friction stir welding parameters on grain size and formability in 5083 aluminum alloy, *Materials Science and Engineering: A*, **456**(1–2): 344–349, 2007, doi: 10.1016/j.msea.2006.12.079.
5. WAN L., HUANG Y., GUO W., LV S., FENG J., Mechanical properties and microstructure of 6082-T6 aluminum alloy joints by self-support friction stir welding, *Journal of Materials Science & Technology*, **30**(12): 1243–1250, 2014, doi: 10.1016/j.jmst.2014.04.009.
6. CAVALIERE P., CAMPANILE G., PANELLA F., SQUILLACE A., Effect of welding parameters on mechanical and microstructural properties of AA6056 joints produced by friction stir welding, *Journal of Materials Processing Technology*, **180**(1–3): 263–270, 2006, doi: 10.1016/j.jmatprotec.2006.06.015.
7. MOHAMMADZADEH JAMALIAN H., FARAHANI M., BESHARATI GIVI M.K., AGHAEI VAFAEI M., Study on the effects of friction stir welding process parameters on the microstructure and mechanical properties of 5086-H34 aluminum welded joints, *The International Journal of Advanced Manufacturing Technology*, **83**(1): 611–621, 2016, doi: 10.1007/s00170-015-7581-5.
8. CAVALIERE P., DE SANTIS A., PANELLA F., SQUILLACE A., Effect of welding parameters on mechanical and microstructural properties of dissimilar AA6082–AA2024 joints produced by friction stir welding, *Materials & Design*, **30**(3): 609–616, 2009, doi: 10.1016/j.matdes.2008.05.044.
9. MISHRA R.S., MA Z.Y., Friction stir welding and processing, *Materials Science and Engineering: R: Reports*, **50**(1–2): 1–78, 2005, doi: 10.1016/j.mser.2005.07.001.
10. LEITÃO C., LOURO R., RODRIGUES D.M., Using torque sensitivity analysis in accessing friction stir welding/processing conditions, *Journal of Materials Processing Technology*, **212**(10): 2051–2057, 2012, doi: 10.1016/j.jmatprotec.2012.05.009.

11. BERNARD D., HATTINGH D.G., Development of high welding speed in friction stir welded 5182-H111, and the resulting influence on down force, *Materials Science Forum*, **828–829**: 366–373, doi: 10.4028/www.scientific.net/MSF.828-829.366.
12. HAMILTON C., KOPYŚCIAŃSKI M., WĘGŁOWSKA A., PIETRAS A., DYMEK S., Modeling, microstructure, and mechanical properties of dissimilar 2017A and 5083 aluminum alloys friction stir welds, *Proceedings of the Institution of Mechanical Engineers, Part B: Journal of Engineering Manufacture*, **233**(2): 553–564, 2019, doi: 10.1177/0954405417740923.
13. SHAH P.H., BADHEKA V.J., Friction stir welding of aluminium alloys: An overview of experimental findings – Process, variables, development and applications, *Proceedings of the Institution of Mechanical Engineers, Part L: Journal of Materials: Design and Applications*, **233**(6): 1191–1226, 2019, doi: 10.1177/1464420716689588.
14. SVENSSON L.-E., KARLSSON L., LARSSON H., KARLSSON B., FAZZINI M., KARLSSON J., Microstructure and mechanical properties of friction stir welded aluminium alloys with special reference to AA 5083 and AA 6082, *Science and Technology of Welding and Joining*, **5**(5): 285–296, 2000, doi: 10.1179/136217100101538335.
15. PALANI K., ELANCHEZHIAN C., SAIPRAKASH K.H.V., SREEKANTH K., DAYANAND D., KUMAR K., KUMAR D., Effect of welding parameters on mechanical properties of dissimilar friction stir processed AA 8011 and AA 5083-H321 aluminium alloys, *IOP Conference Series: Materials Science and Engineering*, **390**(1): 012072, 2018, doi: 10.1088/1757-899X/390/1/012072.
16. MONI V., *Mechanical properties of friction stir welded 5083-H321 and 6082-T651 dissimilar aluminium alloys*, Master Thesis, Cape Peninsula University of Technology, 2020, <https://etd.cput.ac.za/bitstream/20.500.11838/3158/1/Moni.Vuyani.209205520.pdf>.
17. DONG P., LI H.M., SUN D.Q., GONG W.B., LIU J., Effects of welding speed on the microstructure and hardness in friction stir welding joints of 6005A-T6 aluminum alloy, *Materials & Design*, **45**: 524–531, 2013, doi: 10.1016/j.matdes.2012.09.040.
18. THREADGILL P.L., LEONARD A.J., SHERCLIFF H.R., WITHERS P.J., Friction stir welding of aluminium alloys, *International Materials Reviews*, **54**(2): 49–93, 2009, doi: 10.1179/174328009X411136.

Received July 23, 2024; accepted version November 14, 2024.

Online first December 11, 2024.

